MATERIALS SCIENCE

Persistent optical gating of a topological insulator

10.1126/sciadv.1500640

Andrew L. Yeats,[1,2] Yu Pan,[3] Anthony Richardella,[3] Peter J. Mintun,[1] Nitin Samarth,[3] David D. Awschalom[1,2]*

The spin-polarized surface states of topological insulators (TIs) are attractive for applications in spintronics and quantum computing. A central challenge with these materials is to reliably tune the chemical potential of their electrons with respect to the Dirac point and the bulk bands. We demonstrate persistent, bidirectional optical control of the chemical potential of $(Bi,Sb)_2Te_3$ thin films grown on $SrTiO_3$. By optically modulating a space-charge layer in the $SrTiO_3$ substrates, we induce a persistent field effect in the TI films comparable to electrostatic gating techniques but without additional materials or processing. This enables us to optically pattern arbitrarily shaped *p*- and *n*-type regions in a TI, which we subsequently image with scanning photocurrent microscopy. The ability to optically write and erase mesoscopic electronic structures in a TI may aid in the investigation of the unique properties of the topological insulating phase. The gating effect also generalizes to other thin-film materials, suggesting that these phenomena could provide optical control of chemical potential in a wide range of ultrathin electronic systems.

INTRODUCTION

The ability to tune the chemical potential of a material using electric fields—the field effect—is central to semiconductor electronics and is an important degree of freedom in many experiments in solid-state physics. Topological insulators (TIs) have attracted much attention because of their spin-polarized surface and edge states, whose unique coupling of electrical and magnetic properties shows promise for spintronics applications, and whose origin in symmetry gives them quantum-mechanical properties attractive for fundamental research and quantum computing (*1*, *2*). Robust control over the chemical potential of TI materials is important if these states are to be used in new technologies or as a venue for exotic physics. Unfortunately, chemical potential tuning is challenging in TIs because the fabrication of electrostatic top gates tends to degrade material properties (*3*, *4*) and the addition of chemical dopants or adsorbates can cause unwanted disorder (*5*). Advances in materials synthesis have produced alloyed TIs such as $(Bi,Sb)_2Te_3$, whose composition can be tuned to reduce bulk conductivity and position the chemical potential close to the bulk band gap (*6*). However, a dynamic method of tuning the chemical potential is often needed to fully deplete bulk carriers and in experiments where it is necessary to tune precisely to or across the Dirac point.

Much research has focused on controlling the chemical potential of TIs through electrostatic gating (*7*). To this end, $SrTiO_3$ has emerged as a promising dielectric substrate due in part to its extraordinarily high permittivity at low temperature (*8*). This allows a significant field effect to be produced by applying a voltage to the backside of the sample, obviating the need for a top-gate structure. However, back-gating techniques do not provide spatial control of the chemical potential in TI films, which is attractive given the particular importance of edges and interfaces in TI physics. Alternatives to electrostatic gating include the adsorption of gases on TI surfaces (*9*–*11*), electron irradiation (*12*), vacuum deposition of potassium (*13*), contact with organic molecules (*14*), and controlled structural deformation (*15*). Exposure to synchrotron radiation during photoemission experiments can produce changes in the surface band structure of semiconductors (*16*, *17*). These effects have been observed in TIs (*10*, *18*) and recently used to locally adjust surface band bending (*19*). Persistent photodoping has also been observed in a Dirac fermion system based on a HgTe/HgCdTe quantum well (*20*).

RESULTS

We report a bidirectional optical gating effect in thin films of $(Bi,Sb)_2Te_3$ grown by molecular beam epitaxy (MBE) on the (111) face of $SrTiO_3$. Exposure to light with energy above the band gap of $SrTiO_3$ raises the chemical potential of the $(Bi,Sb)_2Te_3$ layer, whereas illumination with lower-energy light reduces it. We attribute this to persistent, optically induced electrical polarization in the $SrTiO_3$ substrate caused by light passing through the semitransparent $(Bi,Sb)_2Te_3$ layer. Figure 1 shows the evolution of the longitudinal resistance of a $(Bi,Sb)_2Te_3/SrTiO_3$ heterostructure under illumination by ultraviolet (UV) or visible light. A series of timed exposures to UV light (λ = 375 nm, I = 1 mW/m^2), interspersed with dark periods, was performed to demonstrate the optical gating effect and its persistence. With each exposure, the longitudinal resistance evolves consistently with a monotonic increase in the chemical potential of the $(Bi,Sb)_2Te_3$ layer. The peak in resistance at t = 1200 s corresponds to the charge neutrality point of the material. At t = 1900 s, a series of lengthening exposures to red light (λ = 635 nm, I = 11.8 W/m^2) reverses this effect. Both effects allow continuous tuning of the chemical potential with illumination dose, though the reason for the differing kinetics is not yet clear. Low optical powers were chosen to produce slow dynamics for clarity of presentation; however, with brighter illumination, samples can be tuned across this range in $\ll$1 s and reproducibly cycled thousands of times. After initial transients, the gating effect shows minimal relaxation for 16 hours (see § S1 in the Supplementary Materials).

To better understand the charge carrier dynamics underlying these resistance changes, we performed Hall effect measurements as a function of both electrostatic gating and UV dose. Figure 2A shows the resistivity and Hall coefficient of a $(Bi,Sb)_2Te_3/SrTiO_3$ heterostructure as a function of the potential applied to the backside of the sample. The sign change of the Hall coefficient indicates the inversion of the majority charge carrier sign. This signifies that the chemical potential has risen

[1]Institute for Molecular Engineering, University of Chicago, Chicago, IL 60637, USA. [2]Department of Physics, University of California, Santa Barbara, Santa Barbara, CA 93106, USA. [3]Department of Physics, Pennsylvania State University, University Park, PA 16802, USA. *Corresponding author. E-mail: awsch@uchicago.edu

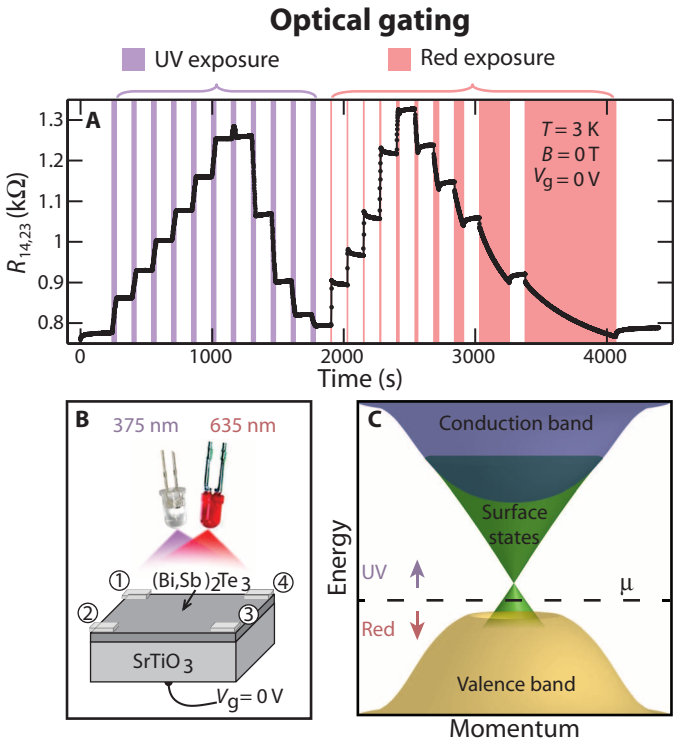

Fig. 1. Persistent optical gating of a TI channel. (**A**) Longitudinal resistance as a function of time during UV and visible illumination. For $t < 1900$ s, a series of 30-s exposures to UV light (purple highlighting), followed by 120-s dark periods, illustrates the optical gating effect and its persistence as the sample's chemical potential is tuned across the charge neutrality point. For $t > 1900$ s, a series of red light exposures (pink highlighting) reverses the effect. The exposure times were chosen for clarity given the differing kinetics of the two effects. The backside of the sample was held at 0 V for the duration of the experiment. (**B**) Schematic of measurement setup, showing Van der Pauw indices of the electrical contacts. (**C**) Schematic of the band structure of $(Bi,Sb)_2Te_3$, showing the effect of optical illumination on the chemical potential μ of the TI layer (dotted line and arrows).

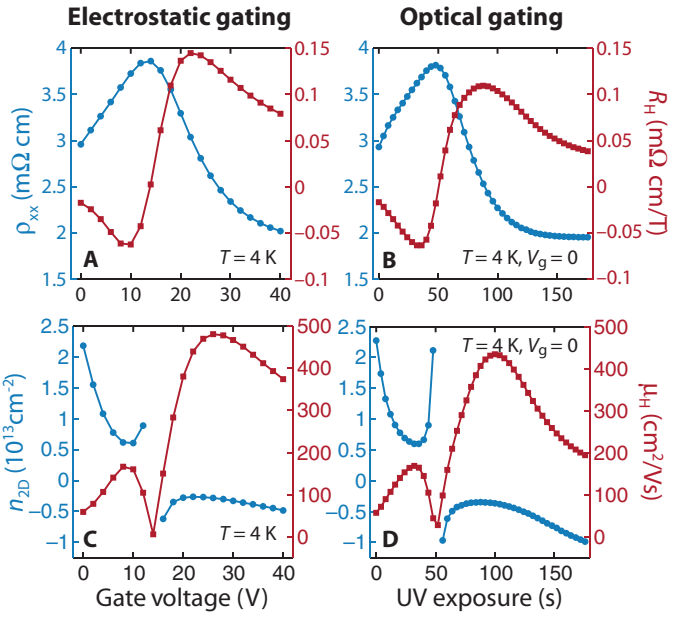

Fig. 2. Charge carrier response to electrostatic and optical gating. (**A**) Longitudinal resistivity ρ_{xx} (blue circles) and Hall coefficient R_H (red squares) as a function of electrostatic back-gating. The peak in resistivity and change in Hall coefficient sign show the ambipolar response of the TI channel. (**B**) Resistivity and Hall coefficient after a series of consecutive timed exposures to UV light, illustrating the optical gating effect. (**C** and **D**) 2D carrier concentration n_{2D} (blue circles) and Hall mobility μ_H (red squares) as a function of optical and electrostatic gating calculated with a one-carrier model. A data point was omitted from (C) and (D) because n_{2D} diverges as $R_H \to 0$ in this model. Data in all plots were collected in the dark at least 60 s after any illumination had ceased.

into the bulk band gap and past the charge neutrality point. The peak in resistivity coincides with the charge carrier inversion, suggesting that the top and bottom surfaces of the film are both effectively gated (*21*). Figure 2B shows the resistivity and Hall coefficient as a function of UV exposure with the backside of the sample held at 0 V. The sample was first initialized by exposure to red light and then subjected to a series of timed exposures to UV light. The longitudinal and Hall resistances were measured at magnetic fields between ±1 T during the dark periods between exposures. A comparable response is seen for both electrostatic and optical gating. The Hall response was linear below 1 T for both types of gating, allowing interpretation with a simple one-carrier model. Figure 2 (C and D) shows the calculated two-dimensional (2D) carrier concentration and Hall mobility. Carrier concentrations below 5×10^{12} cm^{-2} were observed for both types of gating, approaching reported values for the surface states' contribution in this material (*6*). Samples were illuminated from above, so shadowing from the Van der Pauw contacts and surface imperfections may affect the homogeneity of optical gating in this sample, explaining the 10% reduction of peak mobility. When applied together, the optical and electrostatic gating effects superpose with one another (see § S2 in the Supplementary Materials).

A suitable method to control the chemical potential of TIs must not interfere with the unique surface states of these materials. Although not conclusive on its own, one indication of surface state transport is the presence of weak antilocalization (WAL) in magnetoconductance experiments (*8*). Gate-tunable WAL has been reported in TI thin films, and its tunability is attributed to surface-bulk scattering (*22*). Figure 3 shows the magnetoconductance of a $(Bi,Sb)_2Te_3/SrTiO_3$ heterostructure as a function of either optical or electrostatic gating. A zero-field cusp develops as the sample is subjected to positive gate voltage or after consecutive exposures to UV light. This is consistent with the enhancement of WAL as the chemical potential of the TI channel rises above the top of the valence band into the bulk band gap and surface-bulk scattering is reduced. These data demonstrate the suitability of the optical gating effect for the study of coherent carrier effects in TI materials.

$SrTiO_3$ is a host to several optoelectronic effects, which could complicate these data (*23*, *24*). To rule out the influence of substrate conductivity effects, we measured identically prepared bare $SrTiO_3$ substrates at 3 K and at room temperature. Two-terminal resistance measurements exceeded 10 GΩ regardless of the sample's illumination history to UV or visible light, indicating that parallel conduction through the substrate is unlikely to affect our data.

The spectral dependence of optical gating, as well as control experiments with additional materials, shows that the effect originates in the $SrTiO_3$ substrates and is adaptable to other materials systems. Figure 4A shows the longitudinal resistance of a $(Bi,Sb)_2Te_3/SrTiO_3$ heterostructure

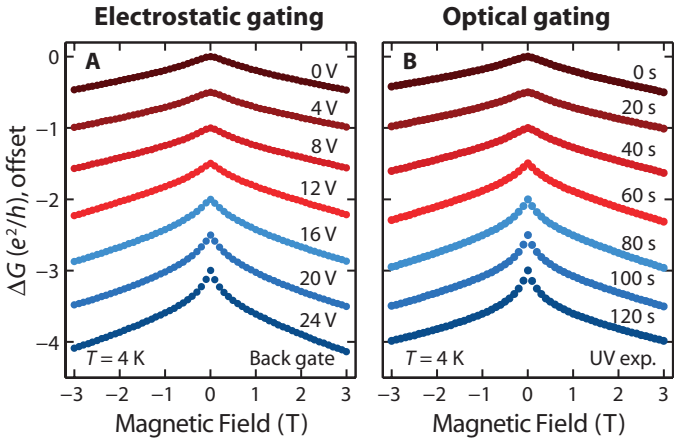

Fig. 3. Optical and electrostatic tuning of WAL. (**A** and **B**) Magnetoconductance ΔG of a $(Bi,Sb)_2Te_3/SrTiO_3$ heterostructure as a function of (A) electrostatic and (B) optical gating. A zero-field cusp develops when the sample is subjected to a positive back-gate voltage or after exposure to UV light. This is consistent with enhancement of WAL as the chemical potential rises above the top of the valence band and surface-bulk scattering is reduced. Qualitatively similar behavior is seen with both gating techniques. Data in all plots were collected in the dark at least 60 s after any illumination had ceased. Data are offset for clarity.

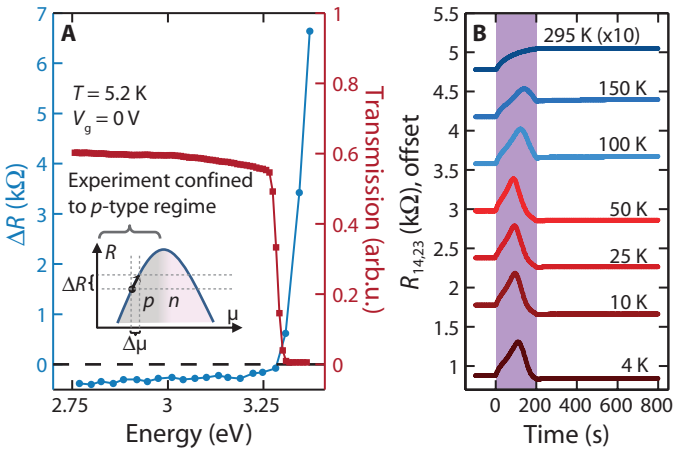

Fig. 4. Spectral and temperature dependence. (**A**) Spectral dependence of the optical gating effect. The relative change in longitudinal resistance ΔR (blue circles) is shown due to identically timed exposures to different energies of light. Before each exposure, red and UV light were used to reset the chemical potential to a similar starting position in the *p*-type regime such that ΔR maps roughly to chemical potential shift $\Delta\mu$ (see inset). The transmission spectrum (red squares) of an identically prepared $SrTiO_3$ substrate is shown for comparison. Both measurements were conducted at 5.2 K. (**B**) Temperature dependence of the optical gating effect, showing its persistence to room temperature. Longitudinal resistance is plotted as a function of time at various temperatures before, during (purple highlighting), and after UV illumination. Traces are offset for clarity. The 295 K trace is multiplied by 10.

before and after timed exposures to different energies of light from a Xe lamp and monochromator. Red and UV light were used before each exposure to initialize the sample to a regime where resistance changes would map monotonically to chemical potential shift (see inset). The sign of the optical gating effect inverts at the band gap energy of $SrTiO_3$, suggesting that the gating effect originates in the $SrTiO_3$ substrate. Measurements of a $(Bi,Sb)_2Te_3$ film grown on InP did not show a bidirectional optical response, indicating that the gating effect we report does not originate from the $(Bi,Sb)_2Te_3$ layer. In contrast, a persistent, bidirectional optical response was observed in a thin film of ZnO grown on $SrTiO_3$, showing that the optical gating effect is applicable to a non-TI material (see § S3 in the Supplementary Materials). These data strongly suggest that the optical gating effect will be adaptable to a wide variety of ultrathin materials grown or deposited on $SrTiO_3$.

A room temperature optical gating effect is desirable for the study of TI physics and devices robust against thermal disorder. Figure 4B shows the temperature dependence of the optical gating effect. The strength of the effect weakens but does not vanish as temperature increases to 295 K. This is roughly consistent with the temperature dependence of the dielectric constant of $SrTiO_3$ (*25*). The 295 K trace is monotonic because optical gating is not strong enough at room temperature to tune this sample through its charge neutrality point. However, optimization of $SrTiO_3$ materials properties might amplify the optical gating effect, increasing its relevance for room temperature applications.

Persistent optical effects are amenable to spatial patterning. By selectively exposing different areas of our samples to measured doses of UV or visible light, we can create arbitrary chemical potential landscapes in a TI channel, which persist for hours after illumination. The bidirectional nature of this effect allows these patterns to be dynamically modified and rewritten in situ, which may be useful for rapid characterization of TI electronic structures. These chemical potential landscapes may be detected with scanning photocurrent microscopy. When electron-hole pairs are photoexcited in a region with a strong chemical potential gradient, they will tend to drift apart. This produces a net photocurrent whose longitudinal component can be detected between the two current leads of a Hall bar. By rastering a laser spot over the surface of a sample while continuously monitoring the zero-bias photocurrent, the gradient of the chemical potential landscape can be imaged.

Photocurrent images of two chemical potential landscapes patterned with the optical gating technique are shown in Fig. 5 (B and C). In each image, the field of view was first initialized *p*-type by exposure to red light. Rectangular *n*-type regions (dotted lines) were defined by projecting UV light onto the sample surface before imaging. Numerical integration of the images was performed to extract the induced chemical potential shifts along the channel, yielding potential profiles consistent with the creation of local *n*-type regions (Fig, 5, D and E). With this technique, arbitrary configurations of *p*- and *n*-type regions can be patterned with a resolution of <20 μm. Exposure to the imaging beam degrades the pattern by *p*-gating the material. However, patterns imaged hours after writing show little evidence of degradation. Spatial potential fluctuations have been reported in photocurrent images of similar $TI/SrTiO_3$ heterostructures (*26*, *27*). The dominance of the patterned photocurrent response observed in our images indicates that optical gating produces chemical potential shifts larger than the intrinsic potential fluctuations present at the length scales accessible to photocurrent microscopy.

DISCUSSION

We propose a defect-mediated mechanism in $SrTiO_3$ to account for the bidirectional optical gating behavior of our samples. Persistent

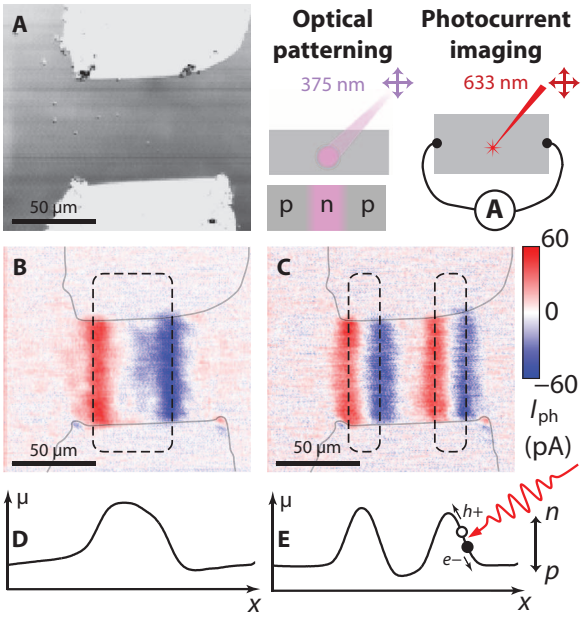

Fig. 5. Writing and imaging *p-n* junctions in a TI. (**A**) Scanning reflectance image of a $(Bi,Sb)_2Te_3$ channel. (**B** and **C**) Photocurrent images of the same region showing the longitudinal component of chemical potential gradients due to *p-n* junctions patterned with the optical gating technique. The channel edges are shown as gray lines for reference. In each image, the field of view was first initialized *p*-type by exposure to red light from a HeNe laser. Rectangular areas (dotted lines) were exposed to UV light before imaging, locally gating these regions *n*-type. UV exposure and photocurrent imaging were repeated, and the images were averaged to reduce noise. (**D** and **E**) Schematics generated by numerical integration of (B) and (C), depicting the chemical potential as a function of lateral position on the channel. The temperature was 5 K.

photorefractive effects in $SrTiO_3$ and other perovskites have been attributed to the optical manipulation of charged defect populations (*28*, *29*). This suggests optical modulation of defect charge states as a means to produce large persistent electric fields in these materials. In our experiments, light with energy above the $SrTiO_3$ bulk band gap penetrates only a short distance past the semitransparent TI layer and into the substrate. Carriers photoexcited from defects near the interface may recombine with states farther into the $SrTiO_3$, where the illumination is weaker, and they will be less likely to be reexcited. This produces a charge asymmetry in the defect population below the interface, growing until all illuminated defects are depopulated, or the induced electric field balances the diffusive pressure set up by the optical gradient. We propose that this field is responsible for the gating effect on the $(Bi,Sb)_2Te_3$ layer. Absent illumination, charges will remain bound in their traps and the gating effect will persist. Alternatively, light with energy below the $SrTiO_3$ bulk band gap reaches defects throughout the substrate volume, allowing isotropic redistribution of charges and the consequent relaxation of the asymmetry. This model qualitatively explains the spectral dependence and persistence of the effect we observe, and is discussed further in § S4 in the Supplementary Materials.

We have demonstrated a persistent, bidirectional optical effect in $SrTiO_3$, which we use to write and erase arbitrary chemical potential landscapes in a TI channel without additional materials or lithography. Photocurrent images of *p-n* junctions patterned with this technique establish that intentional tuning can dominate natural potential fluctuations in this material at length scales accessible to photocurrent microscopy. This optical degree of freedom may facilitate the study of proposed TI phenomena such as topological edge states at *p-n* junctions (*30*, *31*), Klein tunneling (*32*), spin filtering (*33*), bound states outside the Dirac cone (*34*), and Mach-Zehnder interferometry (*35*). Through a procedure of incremental writing and erasing, closed regions gated to different potentials could be moved adiabatically, which may have relevance for proposed methods of quantum computation (*1*, *2*). The optical gating effect is also adaptable to other materials grown or deposited on $SrTiO_3$, suggesting that it may be useful in the study of $LaAlO_3/SrTiO_3$ heterostructures (*36*), graphene (*37*), and transition metal dichalcogenides (*38*, *39*). Persistent optical control of chemical potential may be especially useful for the study of materials incompatible with semiconductor processing techniques or in optical, magnetic, and spectroscopic experiments where electrical contacts are not desirable. The persistence and bidirectionality of the optical gating effect also suggest its potential relevance as a platform for optically defined reconfigurable electronics.

MATERIALS AND METHODS

Samples consist of six quintuple-layers of $(Bi,Sb)_2Te_3$ grown by MBE on $5 \times 5 \times 0.5$–mm (111)–oriented $SrTiO_3$ substrates. The substrates were annealed in oxygen for 2 hours at 875 to 925°C to produce an atomically ordered surface and were screened by atomic force microscopy before growth. Reflection high-energy electron diffraction was performed in situ in the MBE chamber to monitor the growth of the TI films. X-ray diffraction and high-angle annular dark-field scanning transmission electron microscopy were performed after growth to characterize the film crystallinity and interface. Materials characterization data are presented in § S5 in the Supplementary Materials. The $(Bi,Sb)_2Te_3$ film thickness was chosen to avoid hybridization of the top and bottom surface states while remaining thin enough to effectively gate both surfaces (*40*). A Bi:Sb ratio of about 1:1 was chosen to position the chemical potential of the films close to the bulk band gap (*6*). Before gating, all samples showed *p*-type conductivity with a 2D carrier concentration of order 10^{13} cm^{-2}. A control sample was grown on (111)-oriented InP to rule out optical gating effects intrinsic to the $(Bi,Sb)_2Te_3$ material. The MBE growth and characterization of TI materials on $SrTiO_3$ and InP are discussed in detail in a separate article (*41*). Identically prepared bare $SrTiO_3$ substrates were measured to control for substrate photoconductivity. These samples were first annealed in oxygen and then heated to 500°C in the MBE chamber to mimic the thermal history of substrates used for $(Bi,Sb)_2Te_3$ growth. A 50-nm film of ZnO was also sputtered on (111)-oriented $SrTiO_3$ to demonstrate the generalizability of the optical gating effect beyond TI materials (see § S3 in the Supplementary Materials).

Samples grown on $SrTiO_3$ were measured either in the Van der Pauw geometry or after mechanically scratching away the growth layer to form a Hall bar. A Hall bar was patterned on the InP sample with standard photolithography techniques. Except for brief exposure to ambient atmosphere during mounting, samples were kept under vacuum or in a dry nitrogen environment to reduce oxidation. Measurements were conducted in a magneto-optical cryostat. An AC resistance bridge was used to measure Van der Pauw geometry samples. Standard lock-in

techniques were used to measure the Hall bar geometry samples. The excitation current was 30 to 300 nA at 14 to 19 Hz. Electrical contacts to all samples were made with indium and were ohmic. Illumination was provided by commercially available single-color light-emitting diodes or a Xe lamp coupled to a monochromator. Photocurrent images were acquired by rastering a focused HeNe laser spot ($\lambda = 633$ nm, $P = 45$ μW, $d \approx 1$ μm) over the surface of the sample while monitoring the induced zero-bias photocurrent.

SUPPLEMENTARY MATERIALS

Supplementary material for this article is available at http://advances.sciencemag.org/cgi/content/full/1/9/e1500640/DC1

§ S1. Persistence of the optical gating effect for 16 hours.
Fig. S1. Persistence of the optical gating effect for 16 hours.
§ S2. Superposition of electrostatic and optical gating.
Fig. S2. Superposition of electrostatic and optical gating.
§ S3. Optical gating of ≈50-nm sputtered ZnO film on $SrTiO_3$.
Fig. S3. Optical gating of ≈50-nm sputtered ZnO film on $SrTiO_3$.
§ S4. Mechanism of the optical gating effect.
Fig. S4. Mechanism of the optical gating effect.
§ S5. Sample growth and characterization.
Fig. S5. Sample growth and characterization.
References (*42*–*45*)

REFERENCES AND NOTES

1. M. Z. Hasan, C. L. Kane, Colloquium: Topological insulators. *Rev. Mod. Phys.* **82**, 3045–3067 (2010).
2. X.-L. Qi, S.-C. Zhang, Topological insulators and superconductors. *Rev. Mod. Phys.* **83**, 1057–1110 (2011).
3. D. Kong, J. J. Cha, K. Lai, H. Peng, J. G. Analytis, S. Meister, Y. Chen, H.-J. Zhang, I. R. Fisher, Z. X. Shen, Y. Cui, Rapid surface oxidation as a source of surface degradation factor for Bi_2Se_3. *ACS Nano* **5**, 4698–4703 (2011).
4. H. M. Benia, C. Lin, K. Kern, C. R. Ast, Reactive chemical doping of the Bi_2Se_3 topological insulator. *Phys. Rev. Lett.* **107**, 177602 (2011).
5. H. Beidenkopf, P. Roushan, J. Seo, L. Gorman, I. Drozdov, Y. S. Hor, R. J. Cava, A. Yazdani, Spatial fluctuations of helical Dirac fermions on the surface of topological insulators. *Nat. Phys.* **7**, 939–943 (2011).
6. D. Kong, Y. Chen, J. J. Cha, Q. Zhang, J. G. Analytis, K. Lai, Z. Liu, S. S. Hong, K. J. Koski, S.-K. Mo, Z. Hussain, I. R. Fisher, Z.-X. Shen, Y. Cui, Ambipolar field effect in the ternary topological insulator $(Bi_xSb_{1-x})_2Te_3$ by composition tuning. *Nat. Nanotechnol.* **6**, 705–709 (2011).
7. W.-M. Yang, C.-J. Lin, J. Liao, Y.-Q. Li, Electrostatic field effects on three-dimensional topological insulators. *Chin. Phys. B.* **22**, 097202 (2013).
8. J. Chen, H. J. Qin, F. Yang, J. Liu, T. Guan, F. M. Qu, G. H. Zhang, J. R. Shi, X. C. Xie, C. L. Yang, K. H. Wu, Y. Q. Li, L. Lu, Gate-voltage control of chemical potential and weak antilocalization in Bi_2Se_3. *Phys. Rev. Lett.* **105**, 176602 (2010).
9. D. Hsieh, Y. Xia, D. Qian, L. Wray, J. H. Dil, F. Meier, J. Osterwalder, L. Patthey, J. G. Checkelsky, N. P. Ong, A. V. Fedorov, H. Lin, A. Bansil, D. Grauer, Y. S. Hor, R. J. Cava, M. Z. Hasan, A tunable topological insulator in the spin helical Dirac transport regime. *Nature* **460**, 1101–1105 (2009).
10. Y. Xia, D. Qian, D. Hsieh, R. Shankar, H. Lin, A. Bansil, A. V. Fedorov, D. Grauer, Y. S. Hor, R. J. Cava, M. Z. Hasan, Topological control: Systematic control of topological insulator Dirac fermion density on the surface of Bi_2Te_3. arXiv:0907.3089 (2009).
11. P. D. C. King, R. C. Hatch, M. Bianchi, R. Ovsyannikov, C. Lupulescu, G. Landolt, B. Slomski, J. H. Dil, D. Guan, J. L. Mi, E. D. L. Rienks, J. Fink, A. Lindblad, S. Svensson, S. Bao, G. Balakrishnan, B. B. Iversen, J. Osterwalder, W. Eberhardt, F. Baumberger, P. Hofmann, Large tunable Rashba spin splitting of a two-dimensional electron gas in Bi_2Se_3. *Phys. Rev. Lett.* **107**, 096802 (2011).
12. C. W. Rischau, B. Leridon, B. Fauqué, V. Metayer, C. J. van der Beek, Doping of Bi_2Te_3 using electron irradiation. *Phys. Rev. B* **88**, 205207 (2013).
13. Z.-H. Zhu, G. Levy, B. Ludbrook, C. N. Veenstra, J. A. Rosen, R. Comin, D. Wong, P. Dosanjh, A. Ubaldini, P. Syers, N. P. Butch, J. Paglione, I. S. Elfimov, A. Damascelli, Rashba spin-splitting control at the surface of the topological insulator Bi_2Se_3. *Phys. Rev. Lett.* **107**, 186405 (2011).
14. Y. Tanabe, K. K. Huynh, R. Nouchi, S. Heguri, G. Mu, J. Xu, H. Shimotani, K. Tanigaki, Electron and hole injection via charge transfer at the topological insulator $Bi_{2-x}Sb_xTe_{3-y}Se_y$-organic molecule interface. *J. Phys. Chem. C* **118**, 3533–3538 (2014).
15. Y. Okada, W. Zhou, D. Walkup, C. Dhital, S. D. Wilson, V. Madhavan, Ripple-modulated electronic structure of a 3D topological insulator. *Nat. Commun.* **3**, 1158 (2012).
16. M. H. Hecht, Role of photocurrent in low-temperature photoemission studies of Schottky-barrier formation. *Phys. Rev. B Condens. Matter* **41**, 7918–7921 (1990).
17. M. H. Hecht, Time dependence of photovoltaic shifts in photoelectron spectroscopy of semiconductors. *Phys. Rev. B Condens. Matter* **43**, 12102–12105 (1991).
18. A. A. Kordyuk, T. K. Kim, V. B. Zabolotnyy, D. V. Evtushinsky, M. Bauch, C. Hess, B. Büchner, H. Berger, S. V. Borisenko, Photoemission-induced gating of topological insulators. *Phys. Rev. B* **83**, 081303 (2011).
19. E. Frantzeskakis, N. de Jong, B. Zwartsenberg, Y. Huang, T. V. Bay, P. Pronk, E. van Heumen, D. Wu, Y. Pan, M. Radovic, N. C. Plumb, N. Xu, M. Shi, A. de Visser, M. S. Golden, Micro-metric electronic patterning of a topological band structure using a photon beam. arXiv:1412.0822 (2014).
20. P. Olbrich, C. Zoth, P. Vierling, K.-M. Dantscher, G. V. Budkin, S. A. Tarasenko, V. V. Bel'kov, D. A. Kozlov, Z. D. Kvon, N. N. Mikhailov, S. Dvoretsky, S. D. Ganichev, Giant photocurrents in a Dirac fermion system at cyclotron resonance. *Phys. Rev. B* **87**, 235439 (2013).
21. D. Kim, S. Cho, N. P. Butch, P. Syers, K. Kirshenbaum, S. Adam, J. Paglione, M. S. Fuhrer, Surface conduction of topological Dirac electrons in bulk insulating Bi_2Se_3. *Nat. Phys.* **8**, 459–463 (2012).
22. I. Garate, L. Glazman, Weak localization and antilocalization in topological insulator thin films with coherent bulk-surface coupling. *Phys. Rev. B* **86**, 035422 (2012).
23. M. C. Tarun, F. Selim, M. D. McCluskey, Persistent photoconductivity in strontium titanate. *Phys. Rev. Lett.* **111**, 187403 (2013).
24. W. Meevasana, P. D. C. King, R. H. He, S.-K. Mo, M. Hashimoto, A. Tamai, P. Songsiriritthigul, F. Baumberger, Z.-X. Shen, Creation and control of a two-dimensional electron liquid at the bare $SrTiO_3$ surface. *Nat. Mater.* **10**, 114–118 (2011).
25. T. Sakudo, H. Unoki, Dielectric properties of $SrTiO_3$ at low temperatures. *Phys. Rev. Lett.* **26**, 851–853 (1971).
26. C. Kastl, T. Guan, X. Y. He, K. H. Wu, Y. Q. Li, A. W. Holleitner, Local photocurrent generation in thin films of the topological insulator Bi_2Se_3. *Appl. Phys. Lett.* **101**, 251110 (2012).
27. C. Kastl, P. Seifert, X. He, K. Wu, Y. Li, A. Holleitner, Chemical potential fluctuations in topological insulator $(Bi_{0.5}Sb_{0.5})_2Te_3$-films visualized by photocurrent spectroscopy. *2D Mater.* **2**, 024012 (2015).
28. M. E. Guzhva, P. A. Markovin, W. Kleemann, Spontaneous photorefractive effect in $Sr_{1-x}Ca_xTiO_3$ (x=0.014). *Phys. Solid State* **39**, 625–627 (1997).
29. F. Agullo-Lopez, G. F. Calvo, M. Carrascosa, in *Photorefractive Materials and Their Applications I*, vol. 113 of *Springer Series in Optical Sciences*, P. Günter, J.-P. Huignard, Eds. (Springer, New York, 2006), pp. 43–82.
30. T. Yokoyama, A. V. Balatsky, N. Nagaosa, Gate-controlled one-dimensional channel on the surface of a 3D topological insulator. *Phys. Rev. Lett.* **104**, 246806 (2010).
31. J. Wang, X. Chen, B.-F. Zhu, S.-C. Zhang, Topological p-n junction. *Phys. Rev. B* **85**, 235131 (2012).
32. K. M. M. Habib, R. N. Sajjad, A. W. Ghosh, Chiral tunneling of topological states: Towards the efficient generation of spin current using spin-momentum locking. *Phys. Rev. Lett.* **114**, 176801 (2015).
33. G. Liu, G. Zhou, Y.-H. Chen, Modulation of external electric field on surface states of topological insulator Bi_2Se_3 thin films. *Appl. Phys. Lett.* **101**, 223109 (2012).
34. P. Mondal, S. Ghosh, Surface states of a three-dimensional topological insulator in a gate voltage: Conductance oscillation, band structure modification and bands of helical states. arXiv:1411.2091 (2014).
35. R. Ilan, F. de Juan, J. E. Moore, Spin-based Mach-Zehnder interferometry in topological insulator p–n junctions. *Phys. Rev. Lett.* **115**, 096802 (2015).
36. C. Cen, S. Thiel, J. Mannhart, J. Levy, Oxide nanoelectronics on demand. *Science* **323**, 1026–1030 (2009).
37. N. J. G. Couto, B. Sacépé, A. F. Morpurgo, Transport through graphene on $SrTiO_3$. *Phys. Rev. Lett.* **107**, 225501 (2011).
38. Y. Zhang, Q. Ji, G.-F. Han, J. Ju, J. Shi, D. Ma, J. Sun, Y. Zhang, M. Li, X.-Y. Lang, Y. Zhang, Z. Liu, Dendritic, transferable, strictly monolayer MoS_2 flakes synthesized on $SrTiO_3$ single crystals for efficient electrocatalytic applications. *ACS Nano* **8**, 8617–8624 (2014).
39. B. K. Bußmann, K. Marinov, O. Ochedowski, N. Scheuschner, J. Maultzsch, M. Schleberger, Electronic characterization of single-layer MoS_2 sheets exfoliated on $SrTiO_3$. *MRS Proc.* **1474**, mrss12-1474-ccc05-29 (2012).
40. Y. Zhang, K. He, C.-Z. Chang, C.-L. Song, L.-L. Wang, X. Chen, J.-F. Jia, Z. Fang, X. Dai, W.-Y. Shan, S.-Q. Shen, Q. Niu, X.-L. Qi, S.-C. Zhang, X.-C. Ma, Q.-K. Xue, Crossover of the three-dimensional topological insulator Bi_2Se_3 to the two-dimensional limit. *Nat. Phys.* **6**, 584–588 (2010).
41. A. Richardella, A. Kandala, J. S. Lee, N. Samarth, Characterizing the structure of topological insulator thin films. *APL Mater.* **3**, 083303 (2015).
42. T. Hasegawa, S.-i. Mouri, Y. Yamada, K. Tanaka, Giant photo-induced dielectricity in $SrTiO_3$. *J. Phys. Soc. Jpn.* **72**, 41–44 (2003).
43. M. Takesada, T. Yagi, M. Itoh, S. Koshihara, A gigantic photoinduced dielectric constant of quantum paraelectric perovskite oxides observed under a weak DC electric field. *J. Phys. Soc. Jpn.* **72**, 37–40 (2003).

44. M. Takesada, T. Yagi, M. Itoh, T. Ishikawa, S. Koshihara, Photoinduced phenomena in quantum paraelectric oxides by ultraviolet laser irradiation. *Ferroelectrics* **298**, 317–323 (2004).
45. M. B. Klein, in *Photorefractive Materials and Their Applications II*, vol. 114 of *Springer Series in Optical Sciences*, P. Günter, J.-P. Huignard, Eds. (Springer, New York, 2007), pp. 241–285.

Acknowledgments: We thank A. Falk, B. Buckley, D. Christle, C. Nayak, and Y.-S. Chen for useful discussions. We thank J. Jureller and D. Silevitch for assistance with the Hall measurements, and F. Floss for consultation on illumination sources. We acknowledge use of the NSF National Nanofabrication Users Network Facility at Penn State. **Funding:** This work is supported by the Office of Naval Research (grants N00014-12-1-0116 and N00014-12-1-0117), the Air Force Office of Scientific Research Multidisciplinary University Research Initiative (grant FA9550-15-1-0029), the Army Research Office (grant W911NF-12-1-0461), and the NSF Materials Research Science and Engineering Centers (grant NSF-DMR-1420709). **Author contributions:** Y.P. and A.R. grew, fabricated, and characterized the TI materials. A.L.Y., P.J.M., and Y.P. performed the optical experiments. D.D.A. and N.S. supervised the efforts. All of the authors contributed to the analysis of the data, the discussions, and the production of the manuscript. **Competing interests:** The authors declare that they have no competing interests. **Data and materials availability:** All data are presented in the article and Supplementary Materials. Please direct all inquiries to the corresponding author.

Submitted 19 May 2015
Accepted 14 July 2015
Published 9 October 2015
10.1126/sciadv.1500640

Citation: A. L. Yeats, Y. Pan, A. Richardella, P. J. Mintun, N. Samarth, D. D. Awschalom, Persistent optical gating of a topological insulator. *Sci. Adv.* **1**, e1500640 (2015).